Atmospheric
Chemistry
and Physics

Analysis of European ozone trends in the period 1995–2014

Yingying Yan[1,2,3], Andrea Pozzer[1], Narendra Ojha[1,4], Jintai Lin[2], and Jos Lelieveld[1]

[1]Atmospheric Chemistry Department, Max Planck Institute for Chemistry, Mainz, Germany
[2]Laboratory for Climate and Ocean-Atmosphere Studies, Department of Atmospheric and Oceanic Sciences,
School of Physics, Peking University, Beijing 100871, China
[3]Department of Atmospheric Sciences, School of Environmental Studies, China University of Geosciences (Wuhan),
430074, Wuhan, China
[4]Department of Physics, Graphic Era, Dehradun, India

Correspondence: Andrea Pozzer (andrea.pozzer@mpic.de)

Abstract. Surface-based measurements from the EMEP and Airbase networks are used to estimate the changes in surface ozone levels during the 1995–2014 period over Europe. We find significant ozone enhancements (0.20–0.59 μg m^{-3} yr^{-1} for the annual means; P-value < 0.01 according to an F-test) over the European suburban and urban stations during 1995–2012 based on the Airbase sites. For European background ozone observed at EMEP sites, it is shown that a significantly decreasing trend in the 95th percentile ozone concentrations has occurred, especially at noon (0.9 μg m^{-3} yr^{-1}; P-value < 0.01), while the 5th percentile ozone concentrations continued to increase with a trend of 0.3 μg m^{-3} yr^{-1} (P-value < 0.01) during the study period. With the help of numerical simulations performed with the global chemistry-climate model EMAC, the importance of anthropogenic emissions changes in determining these changes over background sites are investigated. The EMAC model is found to successfully capture the observed temporal variability in mean ozone concentrations, as well as the contrast in the trends of 95th and 5th percentile ozone over Europe. Sensitivity simulations and statistical analysis show that a decrease in European anthropogenic emissions had contrasting effects on surface ozone trends between the 95th and 5th percentile levels and that background ozone levels have been influenced by hemispheric transport, while climate variability generally regulated the inter-annual variations of surface ozone in Europe.

1 Introduction

Tropospheric ozone has detrimental effects on human health, and elevated concentrations at the surface are of concern over most of the European region (Hjellbrekke and Solberg, 2002; WHO, 2013; EEA, 2013; Lelieveld et al., 2015). The European Union (EU) Air Quality Directive sets four standards for surface ozone to reduce its impact on human health and crop yields (http://eur-lex.europa.eu/legal-content/EN/TXT/HTML/?uri=CELEX:32008L0050&from=EN, last access: October 2017). These standards are as follows: information threshold (1 h average: 180 μg m^{-3}), alert threshold (1 h average: 240 μg m^{-3}), long-term objective (maximum diurnal 8 h mean: 120 μg m^{-3}), and the target value (long-term objective that should not be exceeded more than 25 days per year, averaged over 3 years). Exceedances are particularly frequent in regions close to high ozone precursor emissions during summer with stagnant meteorological conditions, associated with persistent high temperatures. As a substantial decrease in precursor concentrations has been achieved in Europe in recent decades, the number of exceedances has declined (Guerreiro et al., 2014) in line with a long-term downward trend of pollution emissions (Colette et al., 2011; Wilson et al., 2012). Further, a number of studies have shown that European ozone levels are on average decreasing over the last 20 years (as example, Jonson et al., 2006). Nevertheless, background ozone changes over Europe are not so clear (Wilson et al., 2012), as they are sensitive to climate conditions and intercontinental transport of O_3 and its precursors, and are significant in view of tropo-

spheric chemistry (Lelieveld and Dentener, 2000; Lawrence and Lelieveld, 2010).

The response of surface ozone to a changing climate, with potentially more frequent heat extremes (Bloomer et al., 2009; Jacob and Winner, 2009; Cooper et al., 2012; Fu et al., 2015; Lin et al., 2015; Simon et al., 2015), and concurrent changes in anthropogenic emissions of precursor gases (Bloomer et al., 2009; Fu et al., 2015; Strode et al., 2015; Yan et al., 2018) may pose a challenge for air quality management. Observation and model-based analyses of ozone trends in response to climate change (Bloomer et al., 2009), precursor emissions (Bloomer et al., 2009; Lefohn et al., 2010), and long-range transport (Lin et al., 2015) have been conducted for North America (Strode et al., 2015; Lin et al., 2017; Yan et al., 2018), several Asian regions (Brown-Steiner et al., 2015; Lin et al., 2017), and also for Europe (Meleux et al., 2007; Wilson et al., 2012; Jonson et al., 2006). For Europe, the connection between climate and ozone levels has been the subject of a large number of studies, notably to investigate the effects of climate change on surface ozone levels (Langner et al., 2005, 2012; Meleux et al., 2007; Colette et al., 2011).

Tropospheric ozone is produced photochemically during daytime, mainly from the photolysis of nitrogen dioxide (NO_2), while NO_2 levels are strongly influenced by radicals and their precursors, including organic compounds. Due to the complex photo-chemistry involved, the amount of ozone formed responds nonlinearly to changes in precursor emissions and is sensitive to variations in air temperature, radiation and other climatic factors (Fu et al., 2015; Monks et al., 2015; Coates et al., 2016). Ozone can be destroyed via reaction with NO (i.e., ozone titration) especially during nighttime, and thus a reduction in NO_x emissions could result in more ozone (Jhun et al., 2014; Yan et al., 2018). Previous studies of European ozone have focused on daytime or diurnal mean ozone with little attention paid to the daytime–nighttime contrast in ozone changes (Colette et al., 2011; Wilson et al., 2012; Guerreiro et al., 2014).

Our work contrasts the trends of the monthly 5th and 95th percentile European background ozone levels at hourly levels over the period 1995–2014, based on the hourly ozone measurements from the EMEP network. Additionally, numerical simulations from the global chemistry-climate model ECHAM5/MESSy (EMAC) are conducted to evaluate the model's ability in capturing ozone trends over Europe and to investigate the underlying importance of the meteorology and emission changes for the observed ozone trends.

The manuscript is organized as follows: the observational dataset, model simulations, and analysis methods are described in Sect. 2. In Sect. 3, the average linear trends for the European domain are estimated and analyzed separately for the monthly, seasonal, and annual 5th, 50th, and 95th percentiles of the observed surface ozone concentrations. We then compare the observed ozone trends and variability to results of the atmospheric chemistry – general circulation model EMAC. To investigate the effects of anthropogenic emissions and climate variability on observed European ozone changes, we conduct a sensitivity simulation with constant emissions and statistical analysis with the ERA-Interim 2 m temperature data in Sect. 4. This is followed by the conclusions in Sect. 5.

2 Methods and Data

2.1 Ozone measurements

The hourly ground-level ozone measurements over 1995–2014 have been obtained from the Chemical Coordination Centre of the European Monitoring and Evaluation Programme (EMEP) network (http://www.nilu.no/projects/ccc/emepdata.html, last access: May 2017). Table 1 shows the number of measurement sites (varies from 113 to 137) and the percentage of missing hourly data in each year. Figure 1 shows the site distribution further; as many of the stations were not operating continuously during the study period (Fig. 1), we have only included the sites in the analysis that fulfill the criteria defined by Cooper et al. (2012). Such data selection criteria are applied further, to the US ozone trends analysis with the EPA-AQS measurements by Yan et al. (2018). First, we discard the observational days with less than 66.7 % valid hourly data on any given day or night. Then, we discard any particular season with less than 60 days containing valid data. Finally, for any season, we keep the data with valid seasonal mean ozone over more than 15 years during 1995–2014; otherwise we discard the data in all years for the particular season. Figure 1 shows the selected 93 sites that satisfy the above criteria for analysis.

As the measurements from EMEP network are carried out under the "Co-operative programme for monitoring and evaluation of the long-range transmission of air pollutants in Europe", the monitoring sites are located where there are minimal local influences and consequently the observations are representative of relatively large regions (Tørseth et al., 2012). In order to compare the observed ozone levels and changes over urban, suburban, and rural sites, we also use the hourly measurements over 1995–2012 from the European Environment Agency Airbase system (https://www.eea.europa.eu/data-and-maps/data/airbase-the-european-air-quality-database-8#tab-figures-produced, last access: January 2018; available years: 1973–2012) (Schultz et al., 2017). After applying the same data selection criteria above, we get a total of 685 sites (289 for urban, 150 for suburban, and 246 for rural).

We calculated the linear trends for the European surface ozone at individual hours and mean values for daytime (local time: 07:00–19:00), nighttime (local time: 19:00–07:00), and full days (24 h). For each daytime or nighttime period, the missing data varies between 6.8 and 34.6 % (Table 1). The monthly 5th, 50th, and 95th percentile ozone concen-
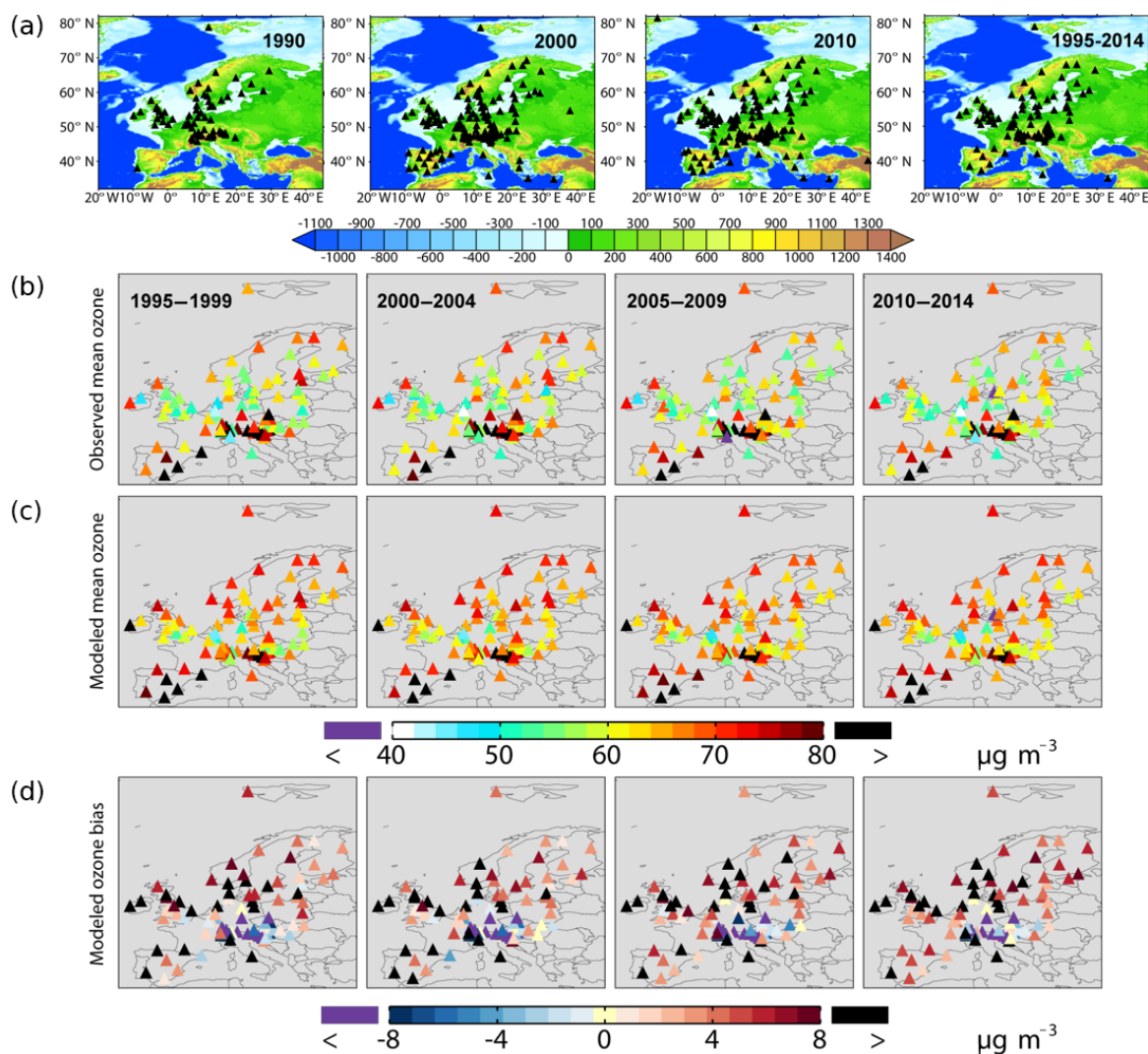
Figure 1. Site distribution **(a)** for the EMEP datasets (1990, 2000, 2010) as well as the selected 93 sites (1995–2014). The overlaid map shows the surface elevation (m) from 2 min Gridded Global Relief Data (ETOPO2v2) available at NGDC Marine Trackline Geophysical database (http://www.ngdc.noaa.gov/mgg/global/etopo2.html, last access: March 2017). The observed **(b)** and modeled **(c)** mean ozone mixing ratios, and also the modeled ozone biases for every five years during 1995–2014 over the selected 93 sites are shown in **(d)**.

trations for each period (per hour, daytime, nighttime, and diurnal) are derived from the lowest, middle, and highest 5th percentile hourly ozone mixing ratios of the corresponding period at individual stations in each month. Averaging over the 93 sites, we then also calculate the trends of different percentile ozone concentrations over the whole Europe.

To calculate the ozone trends per hour, during daytime, nighttime, and per day, we then use the following statistical trend model (Weatherhead et al., 1998; Yoon and Pozzer, 2014):

$$Y_t = \mu + S_t + \omega X_t + N_t,$$

where Y_t denotes the monthly time series of ozone, μ is a constant term representing the offset, $X_t = t/12$ (with t as month) the number of years in the timeseries, and ω is the

magnitude of the trend per year. S_t is a seasonal component in the trend estimates. N_t is the residual term of the interpolation. As the seasonal component does not have much impact on the statistical properties of the estimates of the other terms in the model, we use the deseasonalized monthly data to perform the trend analysis with a model of the following form:

$$Y_t = \mu + \omega X_t + N_t.$$

Using this formulation the linear trends are also analyzed separately for the observed monthly, seasonal and annual surface ozone concentration.

The standard deviation of ozone trends over the European stations is calculated with the following equation:

Table 1. Percentage of missing hourly data from each year in the EMEP station observations.

Year	Number of sites	Missing data		
		Whole day	Daytime	Nighttime
1995	113	32.6 %	30.6 %	34.6 %
1996	115	28.8 %	26.7 %	30.9 %
1997	121	23.9 %	21.6 %	26.2 %
1998	120	18.5 %	16.0 %	21.0 %
1999	127	10.4 %	7.9 %	12.8 %
2000	132	9.8 %	7.2 %	12.3 %
2001	134	11.9 %	9.4 %	14.4 %
2002	136	9.3 %	6.8 %	11.8 %
2003	137	12.1 %	9.8 %	14.4 %
2004	135	10.9 %	8.5 %	13.3 %
2005	132	10.5 %	8.1 %	12.9 %
2006	130	10.6 %	8.1 %	13.1 %
2007	132	9.5 %	7.0 %	12.0 %
2008	136	10.8 %	8.2 %	13.4 %
2009	134	10.6 %	7.8 %	13.3 %
2010	136	15.0 %	12.6 %	17.5 %
2011	135	13.8 %	11.4 %	16.2 %
2012	136	14.1 %	11.8 %	16.4 %
2013	136	19.9 %	17.8 %	22.0 %
2014	137	21.0 %	19.1 %	23.0 %

$$\sigma = \sqrt{\frac{1}{N} \sum_{i=1}^{N} (\omega_i - \alpha)^2},$$

where N is the total number of sites, ω_i is ozone trend at individual sites, and α represents the average ozone trend.

2.2 ERA-Interim 2 m temperature data

To help investigate the underlying effects of climate variability on ozone variations and trends, we relate the monthly variability of ozone to 2 m temperature relevant to the European ground-level meteorology. The 2 m temperature data is from the reanalysis product ERA-Interim, provided by the European Centre for Medium Range Weather Forecast (ECMWF) public datasets web interface (http://apps.ecmwf.int/datasets/, last access: May 2017), covering the data-rich period beginning in 1979 and continuing in real time (Dee et al., 2011). Compared to the ERA-40, the ERA-Interim has improved representation of the hydrological cycle and stratospheric circulation (Dee and Uppala, 2009; Dee et al., 2011). The ERA-Interim atmospheric model and reanalysis system uses cycle 31r2 of ECMWF's Integrated Forecast System (IFS), configured for 60 vertical levels up to 0.1 hPa. The horizontal-spatial resolution is either in a full T255 spectral resolution or in the corresponding N128 reduced Gaussian grid (Dee et al., 2011). ERA-Interim assimilates four analyses per day, at 00:00, 06:00, 12:00, and 18:00 UTC. The ECMWF public website

provides a large variety of data in uniform latitude–longitude grids varying from 0.125 to 3°. Of those, here we analyze the monthly mean 2 m temperature data, which are archived on the 0.75° latitude by 0.75° longitude grid. Additional information (e.g., on current data availability) is available on the ECMWF website at https://www.ecmwf.int/en/forecasts/datasets/archive-datasets/reanalysis-datasets/era-interim (last access: May 2017).

2.3 Atmospheric chemistry modeling

The ECHAM5/MESSy Atmospheric Chemistry (EMAC) model has been used to simulate surface ozone for the 1995–2014 periods. The EMAC model applies the second version of the Modular Earth Submodel System (MESSy2) to link multi-institutional computer codes (Jöckel et al., 2016). The core atmospheric model is the 5th generation European Centre Hamburg general circulation model (ECHAM5) (Roeckner et al., 2006). EMAC simulated gas-phase tracers as well as aerosols have been extensively evaluated in previous studies (e.g., Pozzer et al., 2007, 2012).

In this work, we use the archived RC1SD-base-10a simulation results from the EMAC model conducted by the ESCiMo project (Jöckel et al., 2016). The model results were simulated with version 5.3.02 for ECHAM5 and version 2.51 for MESSy. The archived data were obtained with a T42L90MA spatial resolution, i.e., with a T42 spherical representation which corresponds to a quadratic Gaussian grid with approximately 2.8 latitude by 2.8 longitude, and 90 levels in the vertical, with a top level of up to 0.01 hPa. To reproduce the observed meteorology, the method of Newtonian relaxation towards ERA-Interim reanalysis data (Dee et al., 2011) is applied to weakly nudge the dynamics of the general circulation model. Differently from the work of Jöckel et al. (2016), the model was rerun to cover the full period of measurements and also with a 1-hourly temporal resolution for ozone, in order to compare model results with hourly observational data. We also conducted a sensitivity simulation in which the anthropogenic emissions were kept constant (at the 1994 levels), to represent a scenario with fixed emissions throughout the years where observations are available to investigate the effects of emissions on ozone trends.

The chemical mechanism in the simulations considers the basic gas-phase chemistry of ozone, odd nitrogen, methane, alkanes, alkenes, and halogens (bromine and chlorine). Here we use the Mainz Isoprene Mechanism (version 1; MIM1) to account for the chemistry of isoprene and additional nonmethane hydrocarbons (NMHCs). This mechanism in total includes 310 reactions of 155 species and is included in the submodel MECCA (Jöckel et al., 2010; Sander et al., 2011).

Anthropogenic and biomass burning emissions in the model are incorporated as prescribed sources following the Chemistry-Climate Model Initiative (CCMI) recommendations (Eyring et al., 2013), using the MACCity (Monitoring Atmospheric Composition & Climate/City Zero En-
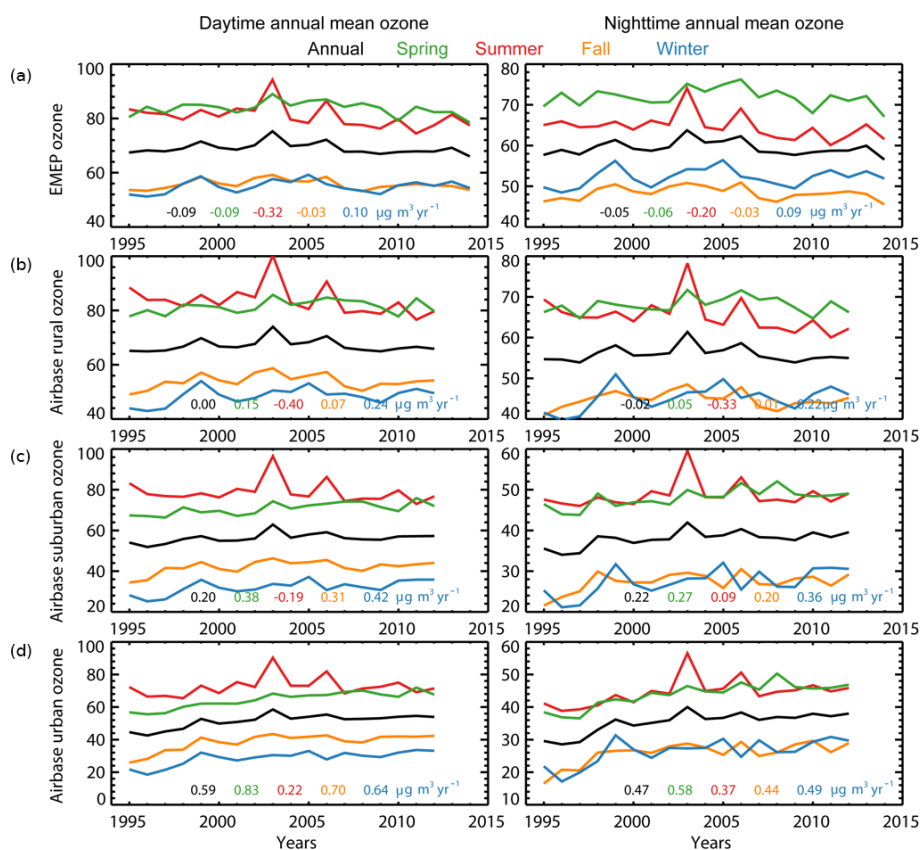
Figure 2. Annual and seasonal mean daytime and nighttime ozone mixing ratios, averaged over the selected sites for EMEP network **(a)**, as well as Airbase network (panel **b** for Airbase rural sites; panel **c** for Airbase suburban sites; and panel **d** for Airbase urban sites). Also shown in each panel are the relevant trends.

ergy) emission inventory, which includes a seasonal cycle (monthly resolved) for biomass burning (Diehl et al., 2012) and anthropogenic emissions (Granier et al., 2011). Additionally, the emissions are vertically distributed as described by Pozzer et al. (2009). Since the total NMVOCs (non-methane volatile organic compounds) values for anthropogenic sectors are not provided by the MACCity raw dataset, they are recalculated from the corresponding species (Jöckel et al., 2016).

Emissions from natural sources have been prescribed as well, either as monthly resolved or annually constant climatology. The spatial and temporal distributions of biogenic NMHCs are based on Global Emissions Initiative (GEIA). In addition, the emissions of terrestrial dimethyl sulfide (DMS), volcanic SO_2, halocarbons, and ammonia are prescribed mostly based on climatologies. The ocean-to-atmosphere fluxes of DMS, C_5H_8, and methanol are calculated by the AIRSEA submodel (Pozzer et al., 2006) following the two-layer model by Liss and Slater (1974). The emissions of soil NO_x (Yienger and Levy, 1995; Ganzeveld et al., 2002) and biogenic isoprene (C_5H_8) (Guenther et al., 1995; Ganzeveld et al., 2002) are calculated online using the submodel ONE-MIS. The lightning NO_x emissions are calculated with the

submodel LNOX (Tost et al., 2007), following the parameterization by Grewe et al. (2001). This scheme links the flash frequency to the thunderstorm cloud updraft velocity. Aerosols are included in the simulation, although their heating rates and surface areas (needed for heterogeneous reactions) are prescribed from an external climatology rather than interactive chemistry. Further details of the model setup on the emissions, physical and chemical processes, as well as the model evaluation with observations can be found in Jöckel et al. (2016).

3 Results

3.1 Ozone trends in EMEP and Airbase measurements

Annual and seasonal mean daytime and nighttime ozone mixing ratios averaged over the EMEP sites and Airbase sites are shown in Fig. 2. Ozone mixing ratios are at their maximum over the spring-to-summer seasons and minimum over the fall-to-winter seasons for different types of station classification. For annual mean ozone, the concentrations, both in daytime and at night, over rural sites (EMEP sites and Airbase rural sites) are higher than those aver-
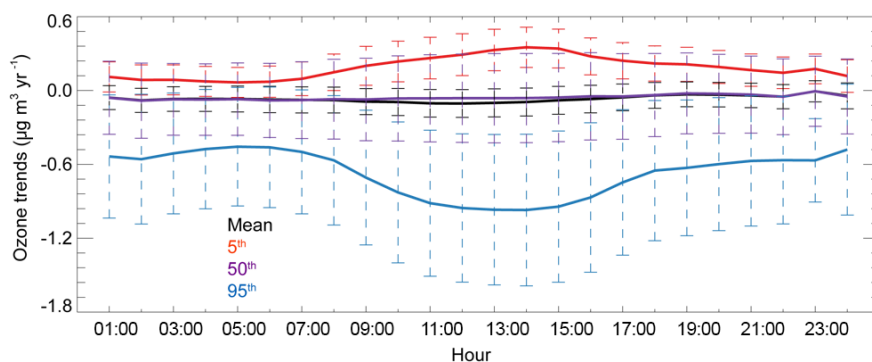
Figure 3. Trend in the observed surface ozone, averaged over Europe, calculated for the selected 93 sites. The black line shows the 1995–2014 linear trends in the deseasonalized European monthly ozone anomalies for each hour of the day (local standard time), the red, purple, and blue lines depict the observed trend for 5th, 50th, and 95th percentile ozone, respectively, and the dashed bars indicate their standard deviations.

aged over the Airbase suburban and urban sites. Although the EMEP (93 sites) ozone and Airbase rural (246 sites) ozone are calculated based on different number of sites, the ozone trends (shown in each panel in Fig. 2) for annual and seasonal means are similar both during daytime and at night. For the Airbase suburban and urban sites, ozone has increased rapidly with the statistically significant growth rates of 0.09–0.83 µg m^{-3} yr^{-1}, except that a decline rate of -0.19 µg m^{-3} yr^{-1} (P-value < 0.01) is also visible for suburban summer ozone during 1995–2012. These suburban and urban ozone enhancements (0.20–0.59 µg m^{-3} yr^{-1} for annual means; P-value < 0.01) are in contrast with the slight rural ozone decrease (-0.09 to -0.02 µg m^{-3} yr^{-1} for annual means; with an increasing trend for winter ozone and a decreasing trend for summer ozone). Similar results of the differences in trend between rural and urban or suburban sites have been shown through a recent study (Chang et al., 2017). As the EMAC model version used here is at a coarse resolution, which is not suitable to investigate the observed contrast ozone trends among the urban, suburban, and rural stations, we focus on the analysis of ozone levels and changes over the regional background areas monitored by EMEP network in the following results.

Figure 3 shows the trends in ozone concentrations (monthly mean, 5th, 50th, and 95th percentile) over EMEP sites during the 1995–2014 period, for each hour of the day. While the average ozone concentrations (and 50th percentiles) do not show significant trends, the 5th and 95th percentile ozone show significant trends with a clear diel cycle. The 95th percentile ozone shows a decreasing trend over Europe during the 1995–2014 period, in which the trend was most pronounced (-0.9 ± 0.5 µg m^{-3} yr^{-1}; P-value < 0.01) during midday (11:00–15:00). 95th percentile ozone concentrations also show a decreasing trend during the night; however, the trends are observed to be smaller (-0.5 ± 0.35 µg m^{-3} yr^{-1}; P-value < 0.01). For the ozone trend of 95th percentile at individual stations, 84 sites (90 %)

are characterized by a decreasing trend in daytime and 78 sites (84 %) at night (Figs. 5 and S2 in the Supplement). Here the standard deviation depicts the variability of the trends among the stations, and therefore reflects the almost homogeneous decrease over entire Europe. Interestingly, in contrast with the 95th percentile, the 5th percentile ozone over Europe shows an increasing trend, especially during midday (0.3 ± 0.16 µg m^{-3} yr^{-1}; P-value < 0.01). Further, the temporal evolutions of ozone anomalies during the 1995–2014 period are shown for 5th and 95th percentile in Fig. S1. The 95th percentile ozone trend indicates a general decline in the photochemical buildup of ozone during noon hours, with the exception of strongly enhanced ozone during 2003. The inter-annual variability is observed to be very large with ozone anomalies in excess of 35 µg m^{-3} in 2003 relative to 2014. For 95th percentile ozone, the sharp increase by up to 20 µg m^{-3} in the year 2003 occurred during a strong European heat wave (Sect. 4.2). The analysis of individual year observations here shows that the increasing trend in the 5th percentile ozone is a robust feature with most of the recent years showing stronger noontime build up in ozone as compared to the 1990s. However, during the study period, the variability in noontime ozone anomalies is lower (~ 10 µg m^{-3}) in the 5th percentile ozone compared to the 95th percentile ozone.

Consistent with the results obtained for hourly ozone, when the observational data is reduced to diurnal values, a growth rate of 0.22 ± 0.15 µg m^{-3} yr^{-1} (P-value < 0.01) is calculated for the European mean 5th percentile ozone, while a stronger decline rate of -0.57 ± 0.34 µg m^{-3} yr^{-1} (P-value < 0.01) is estimated for the European mean 95th percentile ozone (see Table 2). Hereafter we will mainly focus on trends in the daytime mean, nighttime mean, 5th percentile and 95th percentile ozone concentrations.

The observed long-term reduction in 95th percentile ozone concentrations over Europe concurs with the reduction in anthropogenic emissions of ozone precursors (Fig. S6). Anthro-

Table 2. Modeled and observed ozone trends[*] and their standard deviations based on diurnal average European mean ozone concentrations. The mean, 5th, 50th, and 95th percentile represent the monthly statistics of the diurnal averages. The model has been sampled in the same location as the EMEP stations.

	5th percentile	50th percentile	Mean	95th percentile
EMEP ($\mu g\,m^{-3}\,yr^{-1}$)	$0.22^a \pm 0.15$	-0.05 ± 0.23	-0.07 ± 0.21	$-0.57^a \pm 0.34$
EMAC ($\mu g\,m^{-3}\,yr^{-1}$)	$0.42^a \pm 0.14$	0.01 ± 0.10	0.06 ± 0.09	$-0.23^a \pm 0.10$

[*] Trends – [a] P-value < 0.01.

Table 3. Modeled and observed linear trends[*] and their spatial standard deviations of the 1995–2014 European mean annual and seasonal averaged daytime and nighttime mean, as well as their 5th, 50th, and 95th percentile ozone concentrations (averaged over the 93 sites).

	Seasons	Mean		5th percentile		50th percentile		95th percentile	
		EMEP	EMAC	EMEP	EMAC	EMEP	EMAC	EMEP	EMAC
Daytime ($\mu g\,m^{-3}\,yr^{-1}$)	Annual	-0.09 ± 0.24	0.00 ± 0.06	$0.22^a \pm 0.17$	$0.45^a \pm 0.14$	-0.06 ± 0.24	-0.01 ± 0.06	$-0.81^a \pm 0.46$	$-0.48^a \pm 0.15$
	MAM	-0.09 ± 0.27	-0.05 ± 0.08	0.13 ± 0.24	$0.52^a \pm 0.17$	-0.02 ± 0.27	-0.02 ± 0.08	$-0.93^a \pm 0.53$	$-0.49^a \pm 0.16$
	JJA	$-0.32^a \pm 0.24$	-0.10 ± 0.07	-0.03 ± 0.26	$0.41^a \pm 0.20$	$-0.26^a \pm 0.24$	-0.09 ± 0.13	$-1.10^a \pm 0.61$	$-0.54^a \pm 0.16$
	SON	-0.03 ± 0.19	-0.04 ± 0.05	0.09 ± 0.14	$0.36^a \pm 0.12$	-0.04 ± 0.20	-0.02 ± 0.05	$-0.24^a \pm 0.25$	$-0.44^a \pm 0.23$
	DJF	0.10 ± 0.25	$0.18^a \pm 0.14$	$0.25^a \pm 0.15$	$0.39^a \pm 0.22$	0.05 ± 0.27	$0.15^b \pm 0.20$	$-0.28^a \pm 0.31$	-0.08 ± 0.05
Nighttime ($\mu g\,m^{-3}\,yr^{-1}$)	Annual	-0.05 ± 0.23	$0.12^b \pm 0.11$	$0.16^b \pm 0.17$	$0.38^a \pm 0.19$	-0.05 ± 0.24	0.07 ± 0.12	$-0.57^a \pm 0.36$	$-0.21^a \pm 0.10$
	MAM	-0.06 ± 0.29	0.08 ± 0.10	$0.18^b \pm 0.23$	$0.23^a \pm 0.23$	-0.00 ± 0.29	0.04 ± 0.08	$-0.64^a \pm 0.43$	$-0.20^a \pm 0.12$
	JJA	$-0.20^b \pm 0.27$	0.06 ± 0.14	0.07 ± 0.24	$0.36^a \pm 0.22$	-0.15 ± 0.28	0.04 ± 0.14	$-0.71^a \pm 0.52$	$-0.36^a \pm 0.21$
	SON	-0.03 ± 0.21	0.06 ± 0.10	0.05 ± 0.12	$0.19^a \pm 0.16$	-0.05 ± 0.23	0.04 ± 0.11	$-0.21^b \pm 0.24$	$-0.23^a \pm 0.19$
	DJF	0.09 ± 0.24	$0.24^a \pm 0.18$	0.14 ± 0.22	$0.43^a \pm 0.27$	0.06 ± 0.25	$0.20^b \pm 0.25$	$-0.24^b \pm 0.29$	-0.05 ± 0.06

[*] Trends – [a] P-value < 0.01. [b] P-value < 0.05 under an F-test.

pogenic emissions of NO_x and CO over Europe declined by 35 and 58 %, respectively, as calculated from the MACCity inventory. Slower rates of ozone reduction during nighttime are suggested to be combined effects of reduced titration due to lower NO_x emissions, and an increase in the global background ozone concentrations during this period, probably due to growing precursor emissions worldwide since 1995, which has been predicted by Lelieveld and Dentener (2000) based on atmospheric chemistry – transport modeling, and corroborated by satellite observations (Richter et al., 2005; Krotkov et al., 2016). The effect of anthropogenic emissions is discussed in more detail in the Sect. 4.1.

Figure 4 further shows ozone trends for each month of the year. The slight growth rates in the 5th percentile ozone are approximately equally distributed at the level of $0.1 \pm 0.12\,\mu g\,m^{-3}\,yr^{-1}$ (P-value > 0.05), probably due to the absence of ozone diurnal cycle, affected by NO_x anthropogenic emissions, for 5th percentile in winter especially. Conversely, the monthly trends for the 95th percentile ozone are negative with the most rapid decrease rate of $-1.67 \pm 0.4\,\mu g\,m^{-3}\,yr^{-1}$ (P-value < 0.01) in August. For the 50th percentiles (mean) the seasonal cycle of ozone trends declines unevenly from January to August, then picks up in the following months. It leads to the fastest ozone growth in December when the ozone production is minor due to the lowest relative solar UV fluxes and temperatures, and the maximum ozone decline in August, which is the photochemically most active

month in Europe. In December, the 50th (mean) percentile ozone increases at a rate of $0.41 \pm 0.21\,\mu g\,m^{-3}\,yr^{-1}$ ($0.32 \pm 0.09\,\mu g\,m^{-3}\,yr^{-1}$), while a decline rate of $-0.40 \pm 0.24\,\mu g\,m^{-3}\,yr^{-1}$ ($-0.51 \pm 0.13\,\mu g\,m^{-3}\,yr^{-1}$) is calculated in August.

Table 3 shows the trends in European mean (averaged over the 93 sites) seasonal ozone concentrations analyzed separately for daytime and nighttime. The ozone concentrations show pronounced differences in trends over the different seasons. The mean surface ozone in summer, averaged over the selected 93 sites, declines at rates of -0.32 ± 0.24 and $-0.20 \pm 0.27\,\mu g\,m^{-3}\,yr^{-1}$ during day- and nighttime, respectively. It is mainly related to the rapid decline in the highest levels (95th percentile) of ozone with rates of $-1.10 \pm 0.61\,\mu g\,m^{-3}\,yr^{-1}$ (daytime) and $-0.71 \pm 0.52\,\mu g\,m^{-3}\,yr^{-1}$ (nighttime). Although the 95th percentile ozone in spring declines almost as fast as during summer, the decrease in spring for the 95th percentile ozone is compensated by the growth in 5th percentile ozone, leading to much lower decrease rates in spring compared to summer for the mean ozone concentrations. Finally, in winter ozone grows at a rate of $\sim 0.10\,\mu g\,m^{-3}\,yr^{-1}$. This increase occurs mostly in the lower level (5th percentile) ozone concentrations, with growth rates of $0.25 \pm 0.15\,\mu g\,m^{-3}\,yr^{-1}$ (daytime) and $0.14 \pm 0.22\,\mu g\,m^{-3}\,yr^{-1}$ (nighttime).

For the trends in annual mean ozone mixing ratios, a decline in the 95th percentile ozone (daytime: $-0.81 \pm 0.46\,\mu g\,m^{-3}\,yr^{-1}$; nighttime:
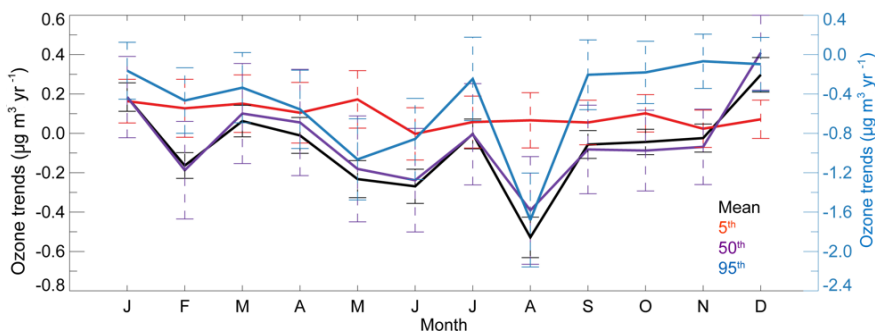
Figure 4. Monthly trend in the observed surface ozone averaged over Europe for the selected 93 sites. The black line shows the 1995–2014 linear trends in the European mean ozone for each month of the year, the red, purple and blue lines depict the observed trend for 5th, 50th, and 95th percentile ozone, respectively, and the dashed bars indicate their standard deviations. The left axis is for the trends of mean, 5th, and 50th percentile ozone, while the right axis is for the 95th percentile ozone.

$-0.57 \pm 0.36\,\mu g\,m^{-3}\,yr^{-1}$) is observed while an increase in the 5th percentile ozone (0.22 ± 0.17 and $0.16 \pm 0.17\,\mu g\,m^{-3}\,yr^{-1}$ for day- and nighttime, respectively, is calculated, resulting in statistically insignificant decreasing trends (daytime: -0.09 ± 0.24; nighttime: $-0.05 \pm 0.23\,\mu g\,m^{-3}\,yr^{-1}$) (Table 3).

Figure 5 further shows the ozone trends distribution site-by-site over the 93 selected stations for daytime mean, 5th, and 95th percentile ozone during the four seasons. The 95th percentile ozone trend shows a decline at most of the selected sites, although ozone increases are also visible at several sites, especially in fall-to-winter. The annual ozone trend averaged over all sites during daytime ($-0.62\,\mu g\,m^{-3}\,yr^{-1}$) is nearly twice that during nighttime ($-0.35\,\mu g\,m^{-3}\,yr^{-1}$, Fig. S2). For the 5th percentile ozone, the annual means have grown over the western and central European sites, in contrast with declines in ozone at other locations over northern and southern Europe. These geographical differences in ozone trends are probably explained by the effects of a general decrease in European anthropogenic precursor emissions, being partly offset by those of climate variability (see Sect. 4.2 for discussion of Figs. 11 and S10). Averaged across all sites, the 5th percentile ozone has grown slightly during daytime as well as at nighttime. The geographical differences in ozone trends are most significant in spring with an average growth rate of $0.01\,\mu g\,m^{-3}\,yr^{-1}$ (Fig. 5). The ozone trends spatial distribution in the daytime (Fig. 5) closely resembles that of the ozone trends in nighttime (Fig. S2) for the mean, 5th percentile, as well as the 95th percentile ozone.

3.2 Ozone exceedance trends

Based on the European directive for ozone concentrations limits, we calculate the number of exceedances for the information threshold and long-term objective (Fig. 6). Averaged over the selected 93 sites, the exceedances of the information threshold as well as the long-term objective have declined at rates of -3.2 and -2.5% per year relative to 1995.

The decrease accelerated after the year 2003, during which a European heat wave raised summer temperatures by 20 to 30 % (in degrees Celsius) compared to the seasonal average over a large part of the continent, extending from northern Spain to the Czech Republic and from Germany to Italy. The variations in the exceedances are inter-annually consistent with the changes in the annual 95th percentile ozone, with a significant correlation coefficient of 0.93 for information threshold exceedances and 0.90 for long-term objective exceedances.

3.3 Ozone trends from EMAC simulation

The same analysis performed on the observations has been carried out on the EMAC model results, i.e., for the same period covered by the observations. To ensure spatiotemporal consistency with the EMEP data, modeled ozone concentrations are sampled at the times and locations of the measurements.

Figure 7 compares the time series of modeled and observed monthly mean ozone over Europe. Although the model overestimates the measurements with a mean bias of $4.3\,\mu g\,m^{-3}$ over the 1995–2014 period, the simulation results are highly correlated with observed ozone, with a significant correlation coefficient of 0.91. The high bias may be explained by the coarse grid resolution of $2.8°$ that was applied, leading to the artificial dispersion of localized NO_x emissions, which optimizes NO_x concentrations over Europe with respect to chemical O_3 formation, also noticed by Jöckel et al. (2016). Such overestimation of the observed ozone due to coarse model horizontal resolution has been reported by Lin et al. (2008) and Yan et al. (2014, 2016). The overestimation after 2010 becomes more evident (mean bias $5.4\,\mu g\,m^{-3}$), mostly due to the emissions used in the model version, being prescribed up to the year 2005 and predicted in the subsequent period. The modeled ozone biases are slightly higher (mean bias: 5.2 and $6.7\,\mu g\,m^{-3}$ for 1995–2014 and 2010–2014, respectively) compared to the
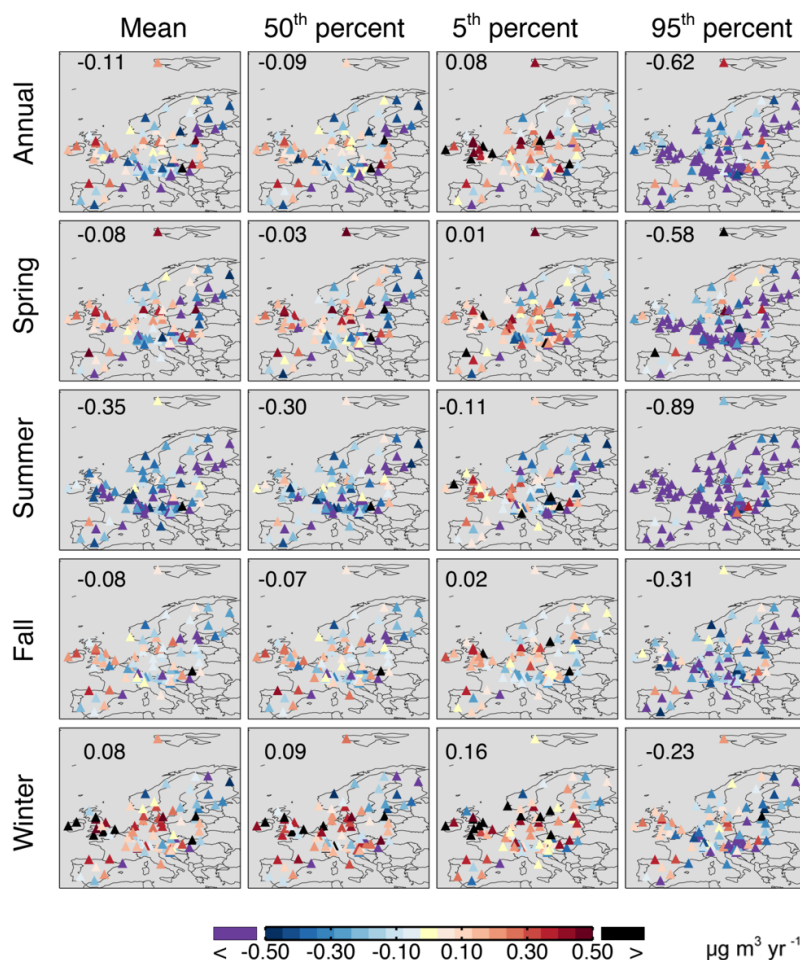
Figure 5. Spatial distribution of measured daytime ozone trends in µg m^{-3} yr^{-1} across the selected 93 sites for average, 5th, 50th, and 95th percentile ozone in annual mean and four seasons. Also shown in each panel are the average trends over all sites.
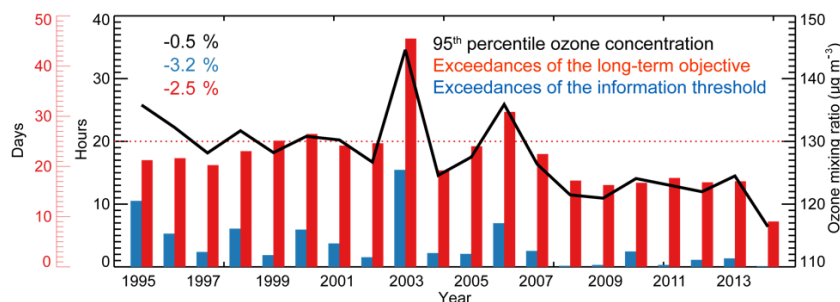

Figure 6. Annual exceedances of the information threshold (for blue bars, hours should be multiplied by 100, 1-hourly averages: 180 µg m^{-3}) as well as the long-term objective (red bars, maximum diurnal 8-hourly mean: 120 µg m^{-3}), compared with the annual 95th percentile ozone concentrations (black line). The red dotted line shows the target value (long-term objective that should not be exceeded more than 25 days per year, averaged over 3 years).

observed de-seasonalized time series. Nevertheless, EMAC model can reproduce the observed inter-annual and seasonal variability of ozone, with statistically significant correlation coefficients at most observation sites. For the diurnal, daytime as well as nighttime mean ozone averaged across the 93

sites, the model-observation correlation is 0.84–0.92 (0.62–0.70 for de-seasonalized time series).

Figure 1 also shows the spatial distribution of observed and modeled mean ozone mixing ratios, as well as the modeled biases for every five years during 1995–2014 over the
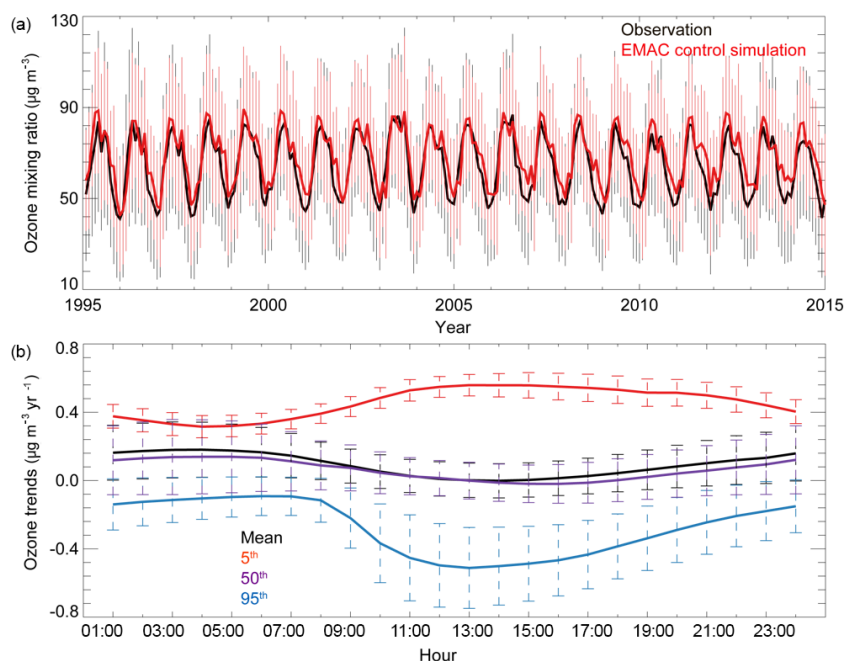
Figure 7. EMAC modeled ozone in $\mu g\,m^{-3}$ over Europe during 1995–2014. Time series of measured (black) and modeled (red) monthly mean ozone over the 93 selected sites **(a)**. Trend in the modeled surface ozone averaged over the selected 93 sites for all hours of the day (local time, **b**). The black line shows the 1995–2014 linear trends in the European mean ozone, the red, purple, and blue lines are the modeled trends for 5th, 50th, and 95th percentile ozone, respectively. The dashed bars indicate their standard deviations.

selected 93 sites. It is shown that for most monitoring stations the model overestimates the observed background ozone concentrations with a bias of up to $15\,\mu g\,m^{-3}$. Ozone overestimation has also been observed in other EMAC simulations when compared to satellite data (Jöckel et al., 2016). Relatively frequent overestimations ($> 10\,\mu g\,m^{-3}$) occur over the coastal and marine sites where the coarse model resolution mixes the polluted air over land with cleaner air masses. Underestimation of modeled ozone also occurs over several sites located at the central Europe. These simulated ozone underestimations are probably due to the underestimation of precursor emissions (especially NO_x) discussed by Oikonomakis et al. (2018).

The EMAC modeled ozone trends per hour are shown in Fig. 7. The agreement with the observationally estimated trends is good, although the model tends to overestimate the trends by 0.12, 0.23, 0.08, and $0.36\,\mu g\,m^{-3}\,yr^{-1}$ for the mean, 5th, 50th, and 95th percentile ozone, respectively. The higher ozone overestimation since 2010 may be the dominant reason for the trend overestimation especially for 95th percentile. The measured diurnal cycle of the ozone trends (Fig. 3) is well captured by the EMAC model for the 5th and 95th percentile ozone concentrations. Consistently, the modeled temporal evolutions (Fig. S3) of annual European 5th percentile ozone anomalies are larger compared to the observations ($\sim 15\,\mu g\,m^{-3}$ versus $\sim 10\,\mu g\,m^{-3}$ enhancements during photochemical buildup of ozone at midday hours during 1990–2014), while being smaller for the 95th

percentile ($\sim 21\,\mu g\,m^{-3}$ versus $\sim 30\,\mu g\,m^{-3}$). Further, the EMAC model reproduces the jump in high level ozone concentrations during the year 2003 that was affected by a major heat wave.

For the diurnal mean values, averaged over Europe, the model produces higher growth rates for the 5th percentile ozone and weaker decrease rates for the 95th percentile ozone compared to the observed trends (Table 2). For the 50th percentile and mean ozone trends averaged over Europe, the model shows statistically insignificant changes, similar to the observed trends (Table 2). Figure S4 further shows the spatial distribution of the simulated diurnal ozone trends. It corroborates that central Europe experiences the highest growth rate for the averaged (also 50th percentile) and 5th percentile ozone concentrations, and the strongest reduction for the 95th percentile ozone during all seasons.

For the trends per month, the EMAC model reproduces the observed variability with statistically significant correlation coefficients of 0.88–0.90 for the mean, 50th and 95th percentile ozone trends (Figs. 4 and S5). Seasonally, for the 95th percentile ozone the modeled ozone trends are much weaker than from measurements in all seasons except the autumn (Table 3). The decreased higher level ozone is probably driven by the anthropogenic ozone precursor emission decline over these years, which has been studied in previous work of ozone change drivers and corroborated in Sect. 4.1 with a sensitivity simulation. For the 5th percentile ozone, especially for the daytime period, the increasing trends are en-
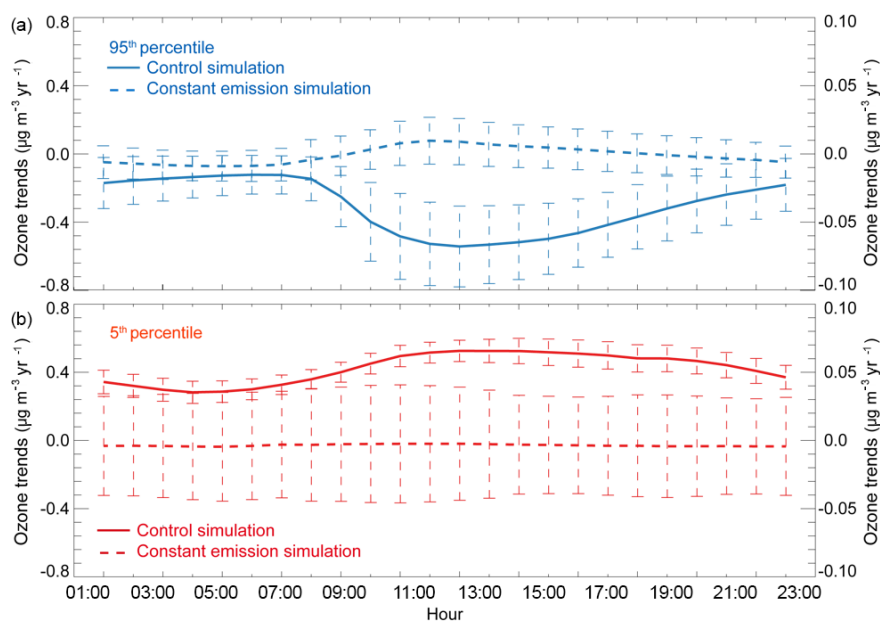
Figure 8. Modeled trend in the surface ozone averaged over the selected 93 sites for all hours of the day (local time). The solid lines (left legends) show the 1995–2014 linear trends in the control simulation for 95th **(a)** and 5th percentile **(b)** ozone, respectively. The dashed lines (right legends) represent the modeled trends by the constant emission simulation. The bars indicate their deviations.

hanced in the model results during all seasons (Table 3). The possible reason for these simulated enhanced ozone trends is the overestimation of the decline of European anthropogenic ozone precursor emissions (decreasing more rapidly than observed) in EMAC.

4 Anthropogenic emissions and climate variability

4.1 Effects of anthropogenic emissions

A sensitivity simulation is conducted with constant global anthropogenic emissions to test the sensitivity of observed European background ozone to inter-annual variability in climate, by removing the effects of anthropogenic emission changes. Consequently, the decline in European emissions (Fig. S6) is removed from the EMAC model. With constant emissions, the modeled ozone shows a slight increase during midday hours for the 95th percentile and a slight decrease for the 5th percentile, in contrast to the trends calculated from the control simulation. In the sensitivity simulations no significant trend (less than $0.1\,\mu g\,m^{-3}\,yr^{-1}$) for any hour of the day is found, and also no contrast in ozone trends between the 5th and 95th percentiles (Fig. 8), which was well reproduced by the control simulation. Therefore, it appears that both the decreases in 95th percentile ozone and the enhancements in 5th percentile ozone are associated with the rapid decline in the precursor gases anthropogenic emissions over Europe, notably of NO_x, prescribed by the MACCity inventory (Fig. S6). These results reflect the effectiveness in controlling high-level ozone, but were unsuccessful in controlling the lower level ozone. Evidently, the 35 % reduction in NO_x emissions in Europe was not sufficient to achieve substantial reductions in ozone, especially of background levels, which are affected by growing emissions in Asia that are transported hemispherically (Lelieveld and Dentener, 2000; Lawrence and Lelieveld, 2010).

Averaging over the selected 93 sites, we calculate the number of exceedances for the information threshold, both in the control and the sensitivity simulation (Fig. 9). In the control simulation, the exceedances of the information threshold have declined at rates of −2.5 % per year relative to 1995, slightly smaller than the observed decrease rate of −3.2 %. The variations in exceedances are inter-annually consistent with the observations, with a significant correlation coefficient of 0.61. However, in the sensitivity simulation, the decline rate (−0.6 %) in the exceedances is much smaller than the rates in the control simulation and in the observations.

By fixing the anthropogenic emissions, ozone trends in each month for the 95th percentile ozone show no obvious decline but rather a slight enhancement with growth rates of −0.23 to $0.50\,\mu g\,m^{-3}\,yr^{-1}$. For the 5th percentile ozone and compared to the control simulation, there is no increase but a slight decrease at a rate of −0.51 to $0.15\,\mu g\,m^{-3}\,yr^{-1}$ in months of the year (Fig. S7). For the trends in annual mean ozone mixing ratios simulated in the sensitivity simulation, an enhancement in the 95th percentile ozone (daytime: $0.16\pm0.18\,\mu g\,m^{-3}\,yr^{-1}$; nighttime: $0.10\pm0.15\,\mu g\,m^{-3}\,yr^{-1}$) is calculated, while a decline in the 5th percentile ozone (-0.11 ± 0.14 and $-0.07\pm0.12\,\mu g\,m^{-3}\,yr^{-1}$ for daytime and nighttime, re-
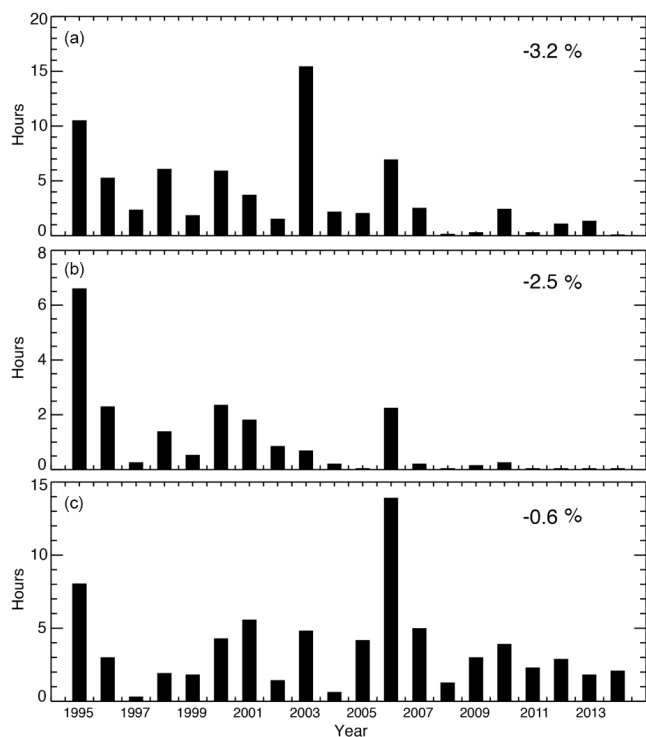
Figure 9. Annual observed (**a**) and modeled (**b**: control simulation; **c**: constant emission simulation) exceedances of the information threshold (1-hourly averages: 180 μg m^{-3}). The hours along the y-axis should be multiplied by 100.

Figure 10. Spatial distribution of the exceedance anomalies in 2003, relevant to the averages over 1995–2002 and for the information threshold as well as the long-term objective, in comparison with the 2 m temperature anomalies in each of the sites.

spectively) is estimated, contrasting with but smaller than the absolute value in the trends of the control simulation. This contrast has been also shown in the trends for each individual hour of the day between the control and sensitivity simulations (Fig. 8). These results show that the effects of decline in anthropogenic emissions on European background ozone change are somewhat offset by the impacts of climate variability. This compensation effect is not only for the high level ozone concentrations, which has been reported by previous studies (Lin et al., 2017), but also for the low level ozone concentrations.

4.2 Effects of climate variability

4.2.1 Heat wave effects

As discussed in number of studies (e.g., Filleul et al., 2006; Vautard et al., 2005; Garcia-Herrera et al., 2010), the 2003 heat waves caused favorable meteorology for ozone buildup, leading to very high ozone concentrations during the summer period (from July to August). Especially, in August 2003, coinciding with a major heat wave in central and northern Europe, massive forest fires were observed from the Terra and MODIS satellite in many parts of Europe, particularly in the south (most pronounced in Portugal and Spain) (Pace et al., 2005; Hodzic et al., 2006, 2007; Solberg et al., 2008).
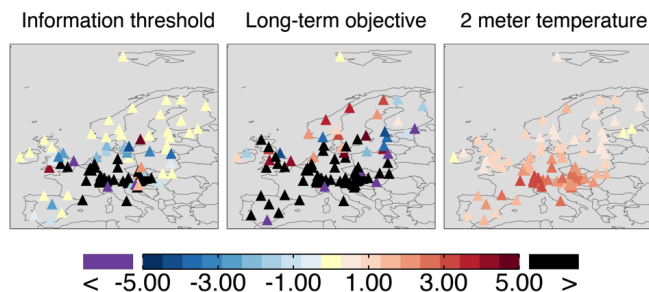
Long-range transport of fire emissions have been found to give rise to significantly elevated air pollution concentration and proved to have contributed to the European ozone peak values in August 2003 (Solberg et al., 2008; Tressol et al., 2008; Ordóñez et al., 2010).

Figure 10 shows the distribution of the difference in the exceedances between 2003 and averaged over 1995–2002 for the information threshold as well as the long-term objective over individual sites. Except for some northern sites, the exceedances in 2003 are much more frequent than the average from 1995 to 2002 over most of the observational sites, especially over central Europe. This exceedance anomaly distribution in 2003 relative to the period of 1995–2002 coincides with the 2 m temperature anomaly distribution, with a statistically significant correlation up to 0.64 (P-value < 0.01 under a T-test; Fig. S8).

4.2.2 Effects of inter-annual climate variability

The exceedance anomaly of information threshold and long-term objective during the year 2003 with respect to the 1995–2002 period follows the anomaly in ozone concentrations, in turn consistent with the temperature anomaly. Figure 11 shows the correlations between the monthly mean 2 m temperature and the monthly mean, 5th, and 95th percentile ozone for diurnal, daytime and nighttime concentrations. Most of these site-by-site correlations are statistically significant (P-value < 0.05 under a T-test; shown as triangles in Fig. 11) with a high fraction (66–91 %) of sites for which significant correlation exists. For each metric (mean and percentiles for diurnal, daytime and nighttime), it corroborates the high correlations over central Europe with statistically significant values up to ∼ 0.82 (P-value < 0.01). It indicates that the surface ozone mixing ratios are highly sensitive to enhanced air temperature, being favorable for photochemical O$_3$ production, which has been reported by previous studies (Lin et al., 2017; Yan et al., 2018 and references therein). For different seasons, ozone variations in fall are most closely affected by temperature (Fig. S9), followed by the spring and summer ozone. The weakest link between ozone and temper-
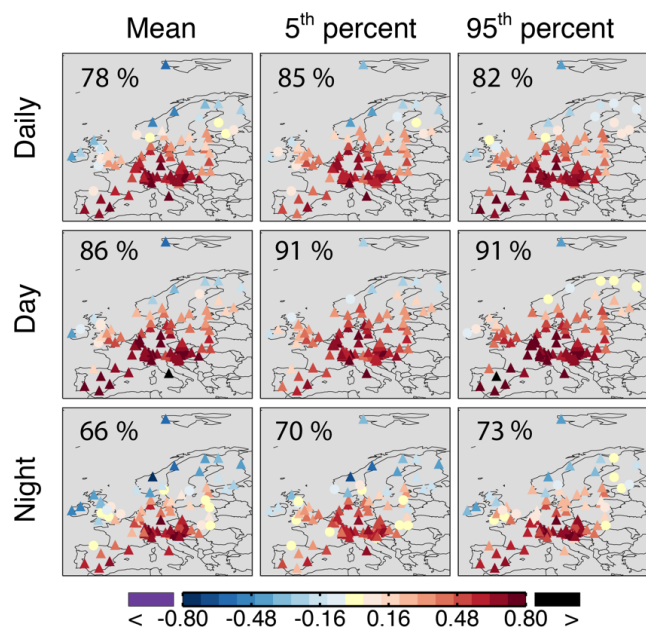
Figure 11. Site-by-site correlations (triangle: P-value < 0.05 under a T-test; circular: P-value > 0.05) between the monthly mean 2 m temperature and monthly mean, 5th, and 95th percentile ozone in the daily data, and during daytime as well as nighttime. Also shown in each panel are the fraction of sites for which significant correlation exists.

ature is in winter with few sites for which significant correlation exists, especially for 95th percentile.

In contrast to the positive correlations over central and southern stations, ozone concentrations over the northern and western sites are negative and significantly correlated with temperature, associated with statistically insignificant correlations at several sites located in the transition regions from positive-correlation to negative-correlation (Fig. 11). This may be related to the influence of the Northern Atlantic Oscillation (NAO; a dominant mode of winter climate variability in the North Atlantic region including Europe; higher correlations with ozone in winter shown in Fig. S11), which had an opposite impact on ozone over northern and western compared to central and southern Europe (Fig. S10). This is because the positive NAO phase is associated with enhanced pressure gradient between the subtropical high pressure center (stronger than usual) and the Icelandic low (deeper than normal). It can result in more and stronger winter storms crossing the Atlantic Ocean on a more northerly pathway, and consequently lead to warm and wet air in northern Europe. Compared to the impact of temperature, the effect of NAO on ozone is relatively modest with much lower correlations (Figs. 11 and S10). The correlations of less than 30 % of the sites pass the significance test (P-value < 0.05). These results underscore that the large-scale climate variability affects the inter-annual variability of European background ozone.

However, in the simulation with constant emissions, the modeled ozone fluctuation of annual European ozone anomalies for individual hours is comparable in magnitude with the results in the control simulation (Fig. S7). In both simulations, the fluctuation dominates around midday for 5th ($\sim 15\,\mu\mathrm{g\,m^{-3}}$ in the base simulation vs. $\sim 13\,\mu\mathrm{g\,m^{-3}}$ in sensitivity simulation) and 95th ($\sim 21\,\mu\mathrm{g\,m^{-3}}$ vs. $\sim 20\,\mu\mathrm{g\,m^{-3}}$) percentile ozone (Figs. S7 and S3). In addition, the variations in the exceedances of the information threshold are inter-annually consistent with the observations and the control simulation, with significant correlation coefficients of 0.54 and 0.56, respectively, comparable to the correlations between observations and control simulation (Fig. 9). Further correlations between the European averaged monthly mean 2 m temperature and the modeled monthly mean (50th), 5th and 95th percentile ozone in the sensitivity simulation are statistically significant with correlation coefficients of 0.69–0.78 for diurnal, daytime, and nighttime concentrations, consistent with the correlations (0.70–0.81) between 2 m temperature and simulated European ozone in the control simulation. These results clearly show that the interannual ozone variations are affected by climate variability.

5 Conclusions and outlook

Based on EMEP observed background ozone in the period 1995–2014, we analyzed the annual and seasonal trends of the mean, the 5th, 50th, and 95th percentile of the ozone concentrations at different temporal distributions, i.e., hourly, diurnal, day- and nighttime. Results show that although reductions in anthropogenic emissions have lowered the peak ozone concentrations (sites with statistically significant trends: 91 out of 93 sites; 98 %), especially during daytime in the period 1995–2014, the lower level ozone concentrations have increased (sites with statistically significant trends: 71 out of 93 sites; 76 %) continually since 1995 over Europe. This leads to insignificant trends in the 50th percentile and mean ozone. Both the 5th and 95th percentile ozone trends follow a diel cycle with the largest trends during periods of strong photochemical activity. These contrasting ozone trends per hour during the day and at different concentration levels are well reproduced by the EMAC chemistry-climate model, although the model slightly overestimates observed ozone at the surface. Furthermore, the number of exceedances of the information threshold and the long-term objective have continuously declined during the 20-year period considered, and the decrease has accelerated since the year 2003.

Sensitivity simulations with constant emissions in the EMAC model, and correlation analysis between modeled ozone and the ERA-Interim 2 m temperature help distinguish effects of climate and anthropogenic emissions on ozone variations and trends. Climate variability generally regulates the interannual variations of European surface ozone, while

the changes in anthropogenic emissions predominantly contribute to ozone trends. However, it appears that the negative ozone trend, due to European emission controls, has been counteracted by a climate related tendency as well as hemispheric dispersion of pollutants from other regions. We note that our analysis over 1995–2014 is a timeframe too short for the analysis of climate tendencies (formally, a 30-year period is necessary). Thus, here the climate related variability is mainly driven by the large-scale processes like NAO and heat wave occurrence, which may be influenced by climate change.

In contrast to the observed diverse trends of European background ozone, significant ozone enhancements are found for the annual means (0.20–$0.59\,\mu g\,m^{-3}\,yr^{-}$) as well as seasonal means (0.09–$0.83\,\mu g\,m^{-3}\,yr^{-1}$), both during daytime and at night over the suburban and urban stations during 1995–2012 based on the Airbase sites. These increasing trends are interesting and should be investigated further in view of the continuous decline in European anthropogenic emissions.

The Supplement related to this article is available online at https://doi.org/10.5194/acp-18-5589-2018-supplement.

References

Bloomer, B. J., Stehr, J. W., Piety, C. A., Salawitch, R. J., and Dickerson, R. R.: Observed relationships of ozone air pollution with temperature and emissions, Geophys. Res. Lett., 36, L09803, https://doi.org/10.1029/2009gl037308, 2009.

Brown-Steiner, B., Hess, P. G., and Lin, M. Y.: On the capabilities and limitations of GCCM simulations of summertime regional air quality: A diagnostic analysis of ozone and temperature simulations in the US using CESM CAM-Chem, Atmos. Environ., 101, 134–148, https://doi.org/10.1016/j.atmosenv.2014.11.001, 2015.

Chang, K.-L., Petropavlovskikh, I., Cooper, O. R., Schultz, M. G., and Wang, T.: Regional trend analysis of surface ozone observations from monitoring networks in eastern North America, Europe and East Asia, Elem. Sci. Anth., 5, 50–71, https://doi.org/10.1525/elementa.243, 2017.

Coates, J., Mar, K. A., Ojha, N., and Butler, T. M.: The influence of temperature on ozone production under varying NO_x conditions – a modelling study, Atmos. Chem. Phys., 16, 11601–11615, https://doi.org/10.5194/acp-16-11601-2016, 2016.

Colette, A., Granier, C., Hodnebrog, Ø., Jakobs, H., Maurizi, A., Nyiri, A., Bessagnet, B., D'Angiola, A., D'Isidoro, M., Gauss, M., Meleux, F., Memmesheimer, M., Mieville, A., Rouïl, L., Russo, F., Solberg, S., Stordal, F., and Tampieri, F.: Air quality trends in Europe over the past decade: a first multi-model assessment, Atmos. Chem. Phys., 11, 11657–11678, https://doi.org/10.5194/acp-11-11657-2011, 2011.

Cooper, O. R., Gao, R.-S., Tarasick, D., Leblanc, T., and Sweeney, C.: Long-term ozone trends at rural ozone monitoring sites across the United States, 1990–2010, J. Geophys. Res.-Atmos., 117, D22307, https://doi.org/10.1029/2012jd018261, 2012.

Dee, D. P. and Uppala, S.: Variational bias correction of satellite radiance data in the ERA-Interim reanalysis, Q. J. Roy. Meteor. Soc., 135, 1830–1841, https://doi.org/10.1002/qj.493, 2009.

Dee, D. P., Uppala, S. M., Simmons, A. J., Berrisford, P., Poli, P., Kobayashi, S., Andrae, U., Balmaseda, M. A., Balsamo, G., Bauer, P., Bechtold, P., Beljaars, A. C. M., van de Berg, L., Bidlot, J., Bormann, N., Delsol, C., Dragani, R., Fuentes, M., Geer, A. J., Haimberger, L., Healy, S. B., Hersbach, H., Holm, E. V., Isaksen, L., Kallberg, P., Koehler, M., Matricardi, M., McNally, A. P., Monge-Sanz, B. M., Morcrette, J. J., Park, B. K., Peubey, C., de Rosnay, P., Tavolato, C., Thepaut, J. N., and Vitart, F.: The ERA-Interim reanalysis: configuration and performance of the data assimilation system, Q. J. Roy. Meteor. Soc., 137, 553–597, https://doi.org/10.1002/qj.828, 2011.

Diehl, T., Heil, A., Chin, M., Pan, X., Streets, D., Schultz, M., and Kinne, S.: Anthropogenic, biomass burning, and volcanic emissions of black carbon, organic carbon, and SO_2 from 1980 to 2010 for hindcast model experiments, Atmos. Chem. Phys. Discuss., 12, 24895–24954, https://doi.org/10.5194/acpd-12-24895-2012, 2012.

EEA: 2013 EEA, Exposure of Ecosystems to Acidification, Eutrophication and Ozone (Indicator CSI 005), available at: http://www.eea.europa.eu/data-and-maps/indicators/exposure-of-ecosystems-to-acidification-2/exposure-of-ecosystems-to-acidification-5 (last access: June 2017), 2013.

Eyring, V., Lamarque, J.-F., Hess, P., Arfeuille, F., Bowman, K., Chipperfield, M., Duncan, B., Fiore, A., Gettelman, A., Gior-

getta, M., Granier, C., Hegglin, M., Kinnison, D., Kunze, M., Langematz, U., Luo, B., Martin, R., Matthes, K., Newman, P., Peter, T., Robock, A., Ryerson, A., Saiz-Lopez, A., Salawitch, R., Schultz, M., Shepherd, T., Shindell, D., Stähelin, J., Tegtmeier, S., Thomason, L., Tilmes, S., Vernier, J.-P., Waugh, D., and Young, P.: Overview of IGAC/SPARC Chemistry-Climate Model Initiative (CCMI) Community Simulations in Support of Upcoming Ozone and Climate Assessments, available at: http://www.sparc-climate.org/fileadmin/customer/6_Publications/Newsletter_PDF/40_SPARCnewsletter_Jan2013_web.pdf (last access: June 2017), 2013.

Filleul, L., Cassadou, S., Médina, S., Fabres, P., Lefranc, A., Eilstein, D., Tertre, A. L., Pascal, L., Chardon, B., Blanchard, M., Declercq, C., Jusot, J., Prouvost, H., and Ledrans, M.: The relation between temperature, ozone, and mortality in nine French cities during the heat wave of 2003, Environ. Health Persp., 114, 1344–1347, 2006.

Fu, T.-M., Zheng, Y., Paulot, F., Mao, J., and Yantosca, R. M.: Positive but variable sensitivity of August surface ozone to large-scale warming in the southeast United States, Nature Climate Change, 5, 454–458, https://doi.org/10.1038/nclimate2567, 2015.

Ganzeveld, L. N., Lelieveld, J., Dentener, F. J., Krol, M. C., Bouwman, A. J., and Roelofs, G. J.: Global soil-biogenic NO_x emissions and the role of canopy processes, J. Geophys. Res.-Atmos., 107, ACH 9-1–ACH 9-17, https://doi.org/10.1029/2001jd001289, 2002.

Garcia-Herrera, R., Diaz, J., Trigo, R. M., Luterbacher, J., and Fischer, E. M.: A review of the European summer heat wave of 2003, Crit. Rev. Environ. Sci. Technol., 40, 267–306, https://doi.org/10.1080/10643380802238137, 2010.

Granier, C., Bessagnet, B., Bond, T., D'Angiola, A., van der Gon, H. D., Frost, G. J., Heil, A., Kaiser, J. W., Kinne, S., Klimont, Z., Kloster, S., Lamarque, J. F., Liousse, C., Masui, T., Meleux, F., Mieville, A., Ohara, T., Raut, J. C., Riahi, K., Schultz, M. G., Smith, S. J., Thompson, A., Aardenne, J., van der Werf, G. R., and van Vuuren, D. P.: Evolution of anthropogenic and biomass burning emissions of air pollutants at global and regional scales during the 1980–2010 period, Climatic Change, 109, 163–190, https://doi.org/10.1007/s10584-011-0154-1, 2011.

Grewe, V., Brunner, D., Dameris, M., Grenfell, J., Hein, R., Shindell, D., and Staehelin, J.: Origin and variability of upper tropospheric nitrogen oxides and ozone at northern midlatitudes, Atmos. Environ., 35, 3421–3433, https://doi.org/10.1016/S1352-2310(01)00134-0, 2001.

Guenther, A., Hewitt, C. N., Erickson, D., Fall, R., Geron, C., Graedel, T., Harley, P., Klinger, L., Lerdau, M., McKay, W. A., Pierce, T., Scholes, B., Steinbrecher, R., Tallamraju, R., Taylor, J., and Zimmerman, P.: A GLOBAL-MODEL OF NATURAL VOLATILE ORGANIC-COMPOUND EMISSIONS, J. Geophys. Res.-Atmos., 100, 8873–8892, https://doi.org/10.1029/94jd02950, 1995.

Guerreiro, C. B. B., Foltescu, V., and de Leeuw, F.: Air quality status and trends in Europe, Atmos. Environ., 98, 376–384, https://doi.org/10.1016/j.atmosenv.2014.09.017, 2014.

Hjellbrekke, A.-G. and Solberg, S.: Ozone measurments 2000, EMEP/CCC-Report 5/2002, 2002.

Hodzic, A., Vautard, R., Chepfer, H., Goloub, P., Menut, L., Chazette, P., Deuzé, J. L., Apituley, A., and Couvert, P.: Evo-

lution of aerosol optical thickness over Europe during the August 2003 heat wave as seen from CHIMERE model simulations and POLDER data, Atmos. Chem. Phys., 6, 1853–1864, https://doi.org/10.5194/acp-6-1853-2006, 2006.

Hodzic, A., Madronich, S., Bohn, B., Massie, S., Menut, L., and Wiedinmyer, C.: Wildfire particulate matter in Europe during summer 2003: meso-scale modeling of smoke emissions, transport and radiative effects, Atmos. Chem. Phys., 7, 4043–4064, https://doi.org/10.5194/acp-7-4043-2007, 2007.

Jacob, D. J. and Winner, D. A.: Effect of climate change on air quality, Atmos. Environ., 43, 51–63, https://doi.org/10.1016/j.atmosenv.2008.09.051, 2009.

Jhun, I., Coull, B. A., Zanobetti, A., and Koutrakis, P.: The impact of nitrogen oxides concentration decreases on ozone trends in the USA, Air Qual. Atmos. Hlth., 8, 283–292, https://doi.org/10.1007/s11869-014-0279-2, 2014.

Jöckel, P., Kerkweg, A., Pozzer, A., Sander, R., Tost, H., Riede, H., Baumgaertner, A., Gromov, S., and Kern, B.: Development cycle 2 of the Modular Earth Submodel System (MESSy2), Geosci. Model Dev., 3, 717–752, https://doi.org/10.5194/gmd-3-717-2010, 2010.

Jöckel, P., Tost, H., Pozzer, A., Kunze, M., Kirner, O., Brenninkmeijer, C. A. M., Brinkop, S., Cai, D. S., Dyroff, C., Eckstein, J., Frank, F., Garny, H., Gottschaldt, K.-D., Graf, P., Grewe, V., Kerkweg, A., Kern, B., Matthes, S., Mertens, M., Meul, S., Neumaier, M., Nützel, M., Oberländer-Hayn, S., Ruhnke, R., Runde, T., Sander, R., Scharffe, D., and Zahn, A.: Earth System Chemistry integrated Modelling (ESCiMo) with the Modular Earth Submodel System (MESSy) version 2.51, Geosci. Model Dev., 9, 1153–1200, https://doi.org/10.5194/gmd-9-1153-2016, 2016.

Jonson, J. E., Simpson, D., Fagerli, H., and Solberg, S.: Can we explain the trends in European ozone levels?, Atmos. Chem. Phys., 6, 51–66, https://doi.org/10.5194/acp-6-51-2006, 2006.

Krotkov, N. A., McLinden, C. A., Li, C., Lamsal, L. N., Celarier, E. A., Marchenko, S. V., Swartz, W. H., Bucsela, E. J., Joiner, J., Duncan, B. N., Boersma, K. F., Veefkind, J. P., Levelt, P. F., Fioletov, V. E., Dickerson, R. R., He, H., Lu, Z., and Streets, D. G.: Aura OMI observations of regional SO_2 and NO_2 pollution changes from 2005 to 2015, Atmos. Chem. Phys., 16, 4605–4629, https://doi.org/10.5194/acp-16-4605-2016, 2016.

Langner, J., Bergström, R., and Foltescu, V.: Impact of climate change on surface ozone and deposition of sulphur and nitrogen in Europe, Atmos. Environ., 39, 1129–1141, 2005.

Langner, J., Engardt, M., Baklanov, A., Christensen, J. H., Gauss, M., Geels, C., Hedegaard, G. B., Nuterman, R., Simpson, D., Soares, J., Sofiev, M., Wind, P., and Zakey, A.: A multi-model study of impacts of climate change on surface ozone in Europe, Atmos. Chem. Phys., 12, 10423–10440, https://doi.org/10.5194/acp-12-10423-2012, 2012.

Lawrence, M. G. and Lelieveld, J.: Atmospheric pollutant outflow from southern Asia: a review, Atmos. Chem. Phys., 10, 11017–11096, https://doi.org/10.5194/acp-10-11017-2010, 2010.

Lefohn, A. S., Shadwick, D., and Oltmans, S. J.: Characterizing changes in surface ozone levels in metropolitan and rural areas in the United States for 1980–2008 and 1994–2008, Atmos. Environ., 44, 5199–5210, https://doi.org/10.1016/j.atmosenv.2010.08.049, 2010.

Lelieveld, J. and Dentener, F. J.: What controls tropospheric ozone?, J. Geophys. Res., 105, 3531–3551, 2000.

Lelieveld, J., Evans, J. S., Fnais, M., Giannadaki, D., and Pozzer, A.: The contribution of outdoor air pollution sources to premature mortality on a global scale, Nature, 525, 367–371, 2015.

Lin, J. T., Youn, D., Liang, X. Z., and Wuebbles, D. J.: Global model simulation of summertime US ozone diurnal cycle and its sensitivity to PBL mixing, spatial resolution, and emissions, Atmos. Environ., 42, 8470–8483, https://doi.org/10.1016/j.atmosenv.2008.08.012, 2008.

Lin, M., Fiore, A. M., Horowitz, L. W., Langford, A. O., Oltmans, S. J., Tarasick, D., and Rieder, H. E.: Climate variability modulates western US ozone air quality in spring via deep stratospheric intrusions, Nat. Commun., 6, 7105, https://doi.org/10.1038/ncomms8105, 2015.

Lin, M., Horowitz, L. W., Payton, R., Fiore, A. M., and Tonnesen, G.: US surface ozone trends and extremes from 1980 to 2014: quantifying the roles of rising Asian emissions, domestic controls, wildfires, and climate, Atmos. Chem. Phys., 17, 2943–2970, https://doi.org/10.5194/acp-17-2943-2017, 2017.

Liss, P. and Slater, P.: Flux of Gases across the Air-Sea Interface, Nature, 247, 181–184, https://doi.org/10.1038/247181a0, 1974.

Meleux, F., Solmonb, F., and Giorgib, F.: Increase in summer European ozone amounts due to climate change, Atmos. Environ., 41, 7577–7587, 2007.

Monks, P. S., Archibald, A. T., Colette, A., Cooper, O., Coyle, M., Derwent, R., Fowler, D., Granier, C., Law, K. S., Mills, G. E., Stevenson, D. S., Tarasova, O., Thouret, V., von Schneidemesser, E., Sommariva, R., Wild, O., and Williams, M. L.: Tropospheric ozone and its precursors from the urban to the global scale from air quality to short-lived climate forcer, Atmos. Chem. Phys., 15, 8889–8973, https://doi.org/10.5194/acp-15-8889-2015, 2015.

Oikonomakis, E., Aksoyoglu, S., Ciarelli, G., Baltensperger, U., and Prévôt, A. S. H.: Low modeled ozone production suggests underestimation of precursor emissions (especially NO_x) in Europe, Atmos. Chem. Phys., 18, 2175–2198, https://doi.org/10.5194/acp-18-2175-2018, 2018.

Ordóñez, C., Elguindi, N., Stein, O., Huijnen, V., Flemming, J., Inness, A., Flentje, H., Katragkou, E., Moinat, P., Peuch, V.-H., Segers, A., Thouret, V., Athier, G., van Weele, M., Zerefos, C. S., Cammas, J.-P., and Schultz, M. G.: Global model simulations of air pollution during the 2003 European heat wave, Atmos. Chem. Phys., 10, 789–815, https://doi.org/10.5194/acp-10-789-2010, 2010.

Pace, G., Meloni, D., and di Sarra, A.: Forest fire aerosol over the Mediterranean basin during summer 2003, J. Geophys. Res., 110, D21202, https://doi.org/10.1029/2005JD005986, 2005.

Pozzer, A., Jöckel, P., Sander, R., Williams, J., Ganzeveld, L., and Lelieveld, J.: Technical Note: The MESSy-submodel AIRSEA calculating the air-sea exchange of chemical species, Atmos. Chem. Phys., 6, 5435–5444, https://doi.org/10.5194/acp-6-5435-2006, 2006.

Pozzer, A., Jöckel, P., Tost, H., Sander, R., Ganzeveld, L., Kerkweg, A., and Lelieveld, J.: Simulating organic species with the global atmospheric chemistry general circulation model ECHAM5/MESSy1: a comparison of model results with observations, Atmos. Chem. Phys., 7, 2527–2550, https://doi.org/10.5194/acp-7-2527-2007, 2007.

Pozzer, A., Jöckel, P., and Van Aardenne, J.: The influence of the vertical distribution of emissions on tropospheric chemistry, Atmos. Chem. Phys., 9, 9417–9432, https://doi.org/10.5194/acp-9-9417-2009, 2009.

Pozzer, A., de Meij, A., Pringle, K. J., Tost, H., Doering, U. M., van Aardenne, J., and Lelieveld, J.: Distributions and regional budgets of aerosols and their precursors simulated with the EMAC chemistry-climate model, Atmos. Chem. Phys., 12, 961–987, https://doi.org/10.5194/acp-12-961-2012, 2012.

Richter, A., Burrows, J. P., Nüss, H., Granier, C., and Niemeier, U.: Increase in tropospheric nitrogen dioxide over China observed from space, Nature, 437, 129–132, 2005.

Roeckner, E., Brokopf, R., Esch, M., Giorgetta, M., Hagemann, S., Kornblueh, L., Manzini, E., Schlese, U., and Schulzweida, U.: Sensitivity of simulated climate to horizontal and vertical resolution in the ECHAM5 atmosphere model, J. Climate, 19, 3771–3791, https://doi.org/10.1175/jcli3824.1, 2006.

Sander, R., Baumgaertner, A., Gromov, S., Harder, H., Jöckel, P., Kerkweg, A., Kubistin, D., Regelin, E., Riede, H., Sandu, A., Taraborrelli, D., Tost, H., and Xie, Z.-Q.: The atmospheric chemistry box model CAABA/MECCA-3.0, Geosci. Model Dev., 4, 373–380, https://doi.org/10.5194/gmd-4-373-2011, 2011.

Schultz, M. G., Schroder, S., Lyapina, O., Cooper, O. R., Galbally, I., Petropavlovskikh, I., von Schneidemesser, E., Tanimoto, H., Elshorbany, Y., Naja, M., Seguel, R. J., Dauert, U., Eckhardt, P., Feigenspan, S., Fiebig, M., Hjellbrekke, A.-G., Hong, Y.-D., Kjeld, P. C., Koide, H., Lear, G., Tarasick, D., Ueno, M., Wallasch, M., Baumgardner, D., Chuang, M.-T., Gillett, R., Lee, M., Molloy, S., Moolla, R., Wang, T., Sharps, K., Adame, J. A., Ancellet, G., Apadula, F., Artaxo, P., Barlasina, M. E., Bogucka, M., Bonasoni, P., Chang, L., Colomb, A., Cuevas-Agullo, E., Cupeiro, M., Degorska, A., Ding, A., Fröhlich, M., Frolova, M., Gadhavi, H., Gheusi, F., Gilge, S., Gonzalez, M. Y., Gros, V., Hamad, S. H., Helmig, D., Henriques, D., Hermansen, O., Holla, R., Hueber, J., Im, U., Jaffe, D. A., Komala, N., Kubistin, D., Lam, K.-S., Laurila, T., Lee, H., Levy, I., Mazzoleni, C., Mazzoleni, L. R., McClure-Begley, A., Mohamad, M., Murovec, M., Navarro-Comas, M., Nicodim, F., Parrish, D., Read, K. A., Reid, N., Ries, L., Saxena, P., Schwab, J. J., Scorgie, Y., Senik, I., Simmonds, P., Sinha, V., Skorokhod, A. I., Spain, G., Spangl, W., Spoor, R., Springston, S. R., Steer, K., Steinbacher, M., Suharguniyawan, E., Torre, P., Trickl, T., Lin, W., Weller, R., Xu, X., Xue, L., and Ma, Z.: Tropospheric Ozone Assessment Report: Database and metrics data of global surface ozone observations, Elementa-Science of the Anthropocene, 5, 58, https://doi.org/10.1525/elementa.244, 2017.

Simon, H., Reff, A., Wells, B., Jia, X., and Frank, N.: Ozone Trends Across the United States over a Period of Decreasing NO_x and VOC Emissions, Environ. Sci. Technol., 49, 186–195, 2015.

Solberg, S., Hov, Ø., Søvde, A., Isaksen, I. S. A., Coddeville, P., De Backer, H., Forster, C., Orsolini, Y., and Uhse, K.: European surface ozone in the extreme summer 2003, J. Geophys. Res., 113, D07307, https://doi.org/10.1029/2007JD009098, 2008.

Strode, S. A., Rodriguez, J. M., Logan, J. A., Cooper, O. R., Witte, J. C., Lamsal, L. N., Damon, M., Van Aartsen, B., Steenrod, S. D., and Strahan, S. E.: Trends and variability in surface ozone over the United States, J. Geophys. Res.-Atmos., 120, 9020–9042, https://doi.org/10.1002/2014jd022784, 2015.

Tressol, M., Ordonez, C., Zbinden, R., Brioude, J., Thouret, V., Mari, C., Nedelec, P., Cammas, J.-P., Smit, H., Patz, H.-W., and Volz-Thomas, A.: Air pollution during the 2003 European heat

wave as seen by MOZAIC airliners, Atmos. Chem. Phys., 8, 2133–2150, https://doi.org/10.5194/acp-8-2133-2008, 2008.

Tørseth, K., Aas, W., Breivik, K., Fjæraa, A. M., Fiebig, M., Hjellbrekke, A. G., Lund Myhre, C., Solberg, S., and Yttri, K. E.: Introduction to the European Monitoring and Evaluation Programme (EMEP) and observed atmospheric composition change during 1972–2009, Atmos. Chem. Phys., 12, 5447–5481, https://doi.org/10.5194/acp-12-5447-2012, 2012.

Tost, H., Jöckel, P., and Lelieveld, J.: Lightning and convection parameterisations – uncertainties in global modelling, Atmos. Chem. Phys., 7, 4553–4568, https://doi.org/10.5194/acp-7-4553-2007, 2007.

Vautard, R., Honoré, C., Beekmann, M., and Rouil, L.: Simulation of ozone during the August 2003 heat wave and emission control scenarios, Atmos. Environ., 39, 2957–2967, https://doi.org/10.1016/j.atmosenv.2005.01.039, 2005.

Weatherhead, E. C., Reinsel, G. C., Tiao, G. C., Meng, X. L., Choi, D. S., Cheang, W. K., Keller, T., DeLuisi, J., Wuebbles, D. J., Kerr, J. B., Miller, A. J., Oltmans, S. J., and Frederick, J. E.: Factors affecting the detection of trends: Statistical considerations and applications to environmental data, J. Geophys. Res.-Atmos., 103, 17149–17161, https://doi.org/10.1029/98jd00995, 1998.

WHO: 2013 WHO, Review of Evidence on Health Aspects of Air Pollution – REVIHAAP Project, Technical Report World Health Organization, Regional Office for Europe, Copenhagen, Denmark, 2013.

Wilson, R. C., Fleming, Z. L., Monks, P. S., Clain, G., Henne, S., Konovalov, I. B., Szopa, S., and Menut, L.: Have primary emission reduction measures reduced ozone across Europe? An analysis of European rural background ozone trends 1996–2005, Atmos. Chem. Phys., 12, 437–454, https://doi.org/10.5194/acp-12-437-2012, 2012.

Yan, Y., Lin, J., Chen, J., and Hu, L.: Improved simulation of tropospheric ozone by a global-multi-regional two-way coupling model system, Atmos. Chem. Phys., 16, 2381–2400, https://doi.org/10.5194/acp-16-2381-2016, 2016.

Yan, Y., Lin, J., and He, C.: Ozone trends over the United States at different times of day, Atmos. Chem. Phys., 18, 1185–1202, https://doi.org/10.5194/acp-18-1185-2018, 2018.

Yan, Y.-Y., Lin, J.-T., Kuang, Y., Yang, D., and Zhang, L.: Tropospheric carbon monoxide over the Pacific during HIPPO: two-way coupled simulation of GEOS-Chem and its multiple nested models, Atmos. Chem. Phys., 14, 12649–12663, https://doi.org/10.5194/acp-14-12649-2014, 2014.

Yienger, J. J. and Levy, H.: EMPIRICAL-MODEL OF GLOBAL SOIL-BIOGENIC NO_X EMISSIONS, J. Geophys. Res.-Atmos., 100, 11447–11464, https://doi.org/10.1029/95jd00370, 1995.

Yoon, J. and Pozzer, A.: Model-simulated trend of surface carbon monoxide for the 2001–2010 decade, Atmos. Chem. Phys., 14, 10465–10482, https://doi.org/10.5194/acp-14-10465-2014, 2014.